Protective Effect of Platinum Nano-antioxidant and Nitric Oxide Against Hepatic Ischemia-Reperfusion Injury

Jing Mu
Peking University
Chunxiao Li
Peking University
Shi Yu
Peking University
Guoyong Liu
Peking University
Jianhua Zou
National University of Singapore
Dong-Yang Zhang
Shenzhen University
Chao Jiang
Shenzhen University
Xiuli Wang
Shenzhen University
Liangcan He
Shenzhen University
Peng Huang
Shenzhen University https://orcid.org/0000-0003-3651-7813
Yuxin Yin
Institute of Systems Biomedicine, Department of Pathology, School of Basic Medical Sciences, Peking-Tsinghua Center for Life Sciences, Peking University Health Science Center https://orcid.org/0000-0003-4102-0043
Xiaoyuan Chen (chen.shawn@nus.edu.sg)
National University of Singapore https://orcid.org/0000-0002-9622-0870

Article

Keywords: hepatic ischemia-reperfusion injury, liver surgery and transplantation, multifunctional nanotherapeutics

Posted Date: July 13th, 2021

DOI: https://doi.org/10.21203/rs.3.rs-660251/v1

Version of Record: A version of this preprint was published at Nature Communications on May 6th, 2022.
See the published version at https://doi.org/10.1038/s41467-022-29772-w.

Abstract

Specific therapeutic interventions of hepatic ischemia-reperfusion injury (IRI) to attenuate liver dysfunction or multiple organ failure following liver surgery and transplantation remain a key concern. Here we present an innovative strategy by integrating a platinum nanoantioxidant and nitric oxide synthase (iNOS) into the zeolitic imidazolate framework-8 (ZIF-8)-based hybrid nanoreactor for effective prevention of IRI. Platinum nanoantioxidant could scavenge excessive reactive oxygen species (ROS) at the injury site and meanwhile generate oxygen for subsequent synthesis of nitric oxide (NO) under the catalysis of iNOS. Such cascade reaction successfully achieved dual protection for the liver through ROS clearance and NO regulation, remarkably enabling reduction of oxidative stress, inhibition of macrophage activation and neutrophil recruitment, and ensuing suppression of proinflammatory cytokines. The current work establishes a proof of concept of multifunctional nanotherapeutics against IRI, which may provide a promising intervention solution in clinical use.

Introduction

Currently, liver resection and transplantation have been widely used in the clinic to treat various liver diseases such as intrahepatic bile duct stones, liver trauma, tumors and other diseases[1]. During the surgery, liver ischemia reperfusion injury (IRI) occurs due to the cessation and restoration of blood supply, which may result in an acute inflammatory response, severe liver damage, and even multiple organ failure and death[2–4]. Current intervention strategies for hepatic IRI include ischemic preconditioning, pharmacological agents preconditioning, gene therapy, and so on[5,6]. However, due to the complicated pathophysiological processes of IRI, there are still lack of effective solutions for the prevention and intervention of IRI in the clinic, so far.

Hepatic IRI is a pathological process involving multiple factors, including acidosis, oxidative stress, intracellular calcium overload, and activation of macrophages and neutrophils caused by hypoxic metabolism[2,7]. Pharmacological interventions such as supplementation of antioxidants to reduce the oxidative stress have be explored to minimize the risk of liver damage[8–10]. Recently, accumulating evidence reveals that nitric oxide (NO) plays diverse roles in modulating cell behaviors and NO-releasing materials have be designed for potential therapeutic applications[11–15]. In particular, it has been reported that the administration of inhaled NO, nitrite or NO donor drugs could attenuate ischemia/reperfusion injury during the liver surgery and accelerate the restoration of liver function[16–18]. However, challenges such as short half-life of NO, toxic side effect and drug tolerance remain and further improvements are needed[14].

Since the discovery of Fe_3O_4 nanoparticles as the peroxidase mimics[19], a variety of nanomaterials capable of mimicking the functions of natural enzymes, namely nanozymes, have attracted considerate interest[20–22]. Owing to advantages in stability, low cost, and recyclability, nanozymes have been widely used in areas of chemistry, biology, and medicine[23–26]. Among these nanozymes, several nanomaterials

have displayed promising effect on the elimination of reactive oxygen species (ROS), which could be employed as biomimetic antioxidants to regulate ROS homeostasis[25,27–30]. In addition, nanozyme-catalyzed cascade reactions are becoming intriguing for versatile biomedical applications[31–34]. For example, Li *et al* integrated the artificial Au nanoparticle (NP) nanozyme and natural ATP synthase into hollow silica microspheres for mitochondria-mimicking oxidative phosphorylation[31]. In the designed natural-artificial hybrid architecture, the Au NPs could convert glucose into gluconic acid in the presence of oxygen (O_2) and the resulting transmembrane proton gradient facilitated the production of ATP catalyzed by ATP synthase. Nanozyme-involved cascade reactions exhibit great benefits in reducing the diffusion barriers, minimizing intermediate decomposition and enhancing local concentrations of reactants, thereby improving the intercommunication and efficiency of catalytic reactions[33,34].

Given the endogenous synthesis of NO produced from □-Arginine (□-Arg) by the catalysis of nitric oxide synthases (NOS), herein, we rationally designed a nanozyme-containing biomimetic cascade system to achieve simultaneous NO generation and noxious ROS depletion for effective prevention of IRI. To make full use of the inherent advantages of nanozymes and natural enzymes, ultrasmall platinum nanoparticles (Pt NPs) with superoxide dismutase/catalase-like properties and induced nitric oxide synthase (iNOS) are integrated into the zeolitic imidazolate framework-8 (ZIF-8) carriers to form a safe and effective nanoreactor (Pt-iNOS@ZIF). By virtue of ROS produced in the process of hepatic IRI as the reactant, the Pt NPs nanozyme could not only achieve effective ROS elimination, but also result in a huge amount of oxygen (O_2) generation, which further promotes the production of NO *via* the catalysis of iNOS in the presence of □-Arg (Fig. 1a). With the aid of Pt-iNOS@ZIF, the whole process can greatly reduce oxidative stress-induced damage, inhibit cell apoptosis and reduce the expression of proinflammatory cytokines, leading to effective intervention of hepatic IRI (Fig. 1b). Overall, the designed nanoractor not only improves the targeting and bioavailability of NO, but also exhibits dual protective effects *via* ROS elimination and NO modulation, thereby offering a promising strategy to prevent the liver from IRI.

Results

Design, synthesis, and characterization of Pt-iNOS@ZIF. In this study, the natural-artificial hybrid nanoreactor was designed and synthesized. First, ultrasmall polyvinylpyrrolidone-coated Pt NPs were successfully synthesized according to the reported method[35]. Then the co-precipitation approach was applied to simultaneously embed enzyme molecules (iNOS) and Pt NPs into the ZIF-8 supporting matrix (Fig. 2a). Transmission electron microscopy (TEM) and elemental mapping results clearly indicated that the obtained Pt NPs had an average size of ~ 3 nm with a narrow size distribution. Interestingly, the Pt NPs could be effectively deposited in the whole ZIF-8 NPs during the co-precipitation process (Fig. 2b-d). The as-prepared Pt-iNOS@ZIF displayed an average size distribution of 99.7 ± 9.0 nm by dynamic light scattering (DLS) measurement (Fig. 2e). Next, TEM results suggested the loading content of Pt element gradually increased with the increasing feeding amount of Pt NPs (Pt:Zn ratios of 1:250, 1:50, and 1:10) (**Supplementary Fig. S1**). The optimal loading content of Pt in Pt-iNOS@ZIF with well dispersibility in aqueous solutions was calculated to be 2.3% (wt %) by inductively coupled plasma-optical emission

spectrometry (ICP-OES). To investigate the enzyme-mediated biomimetic mineralization processes, the iNOS@ZIF NPs were synthesized, which displayed similar morphology with ZIF-8 NPs. X-ray diffraction (XRD) pattern suggested no significant difference in the crystal structure before and after the enzyme encapsulation (Fig. 2f and **Supplementary Fig. S2**). In addition, Fig. 2g showed that there were close zeta potential values before and after the iNOS encapsulation, further validating the enzyme embedding, rather than surface absorption processes[36]. The zeta potential of Pt-iNOS@ZIF-8 was about 8.6 mV and its favored dispersibility in aqueous solutions with maximum loading content of iNOS up to 6.8 wt% is promising for further *in vivo* applications.

***In vitro* performance.** Firstly, the enzyme-like catalytic activities of Pt NPs were examined by superoxide dismutase (SOD) activity assay kit and hydrogen peroxide assay kit, respectively. SOD is known to catalyze the superoxide anion ($\bullet O_2^-$) to generate oxygen (O_2) and hydrogen peroxide (H_2O_2), while catalase (CAT) is able to decompose H_2O_2 into H_2O and O_2. By following the commercially available standard protocols, the inhibition rate of $\bullet O_2^-$ and H_2O_2 was obtained. Results demonstrated the elimination ability of both $\bullet O_2^-$ and H_2O_2 increased with the increase of Pt NPs concentrations (Fig. 3a, 3b). To further verify the SOD/CAT mimic capability, the time course of O_2 generation was monitored by dissolved oxygen probe. In the presence of Pt NPs, the O_2 level gradually increased over time and the addition of more Pt NPs would undoubtedly accelerate the generation of O_2 (Fig. 3c). Moreover, the Michaelis-Menten constant (K_M) and maximum velocity (V_{max}) were determined to be 172 mM and 3.46×10^{-6} M s^{-1}, given the Michaelis-Menten curves and Lineweaver-Burk plot (Fig. 3d, 3e). Taken together, these results clearly demonstrated that Pt NPs exerted both superior SOD and CAT-like activities, enabling effective elimination of $\bullet O_2^-$ and H_2O_2.

Given the consumption of O_2 during the synthesis of NO, we subsequently evaluated whether the generated O_2 could continuously promote the oxidization of □-Arg into NO. Compared to Pt@ZIF and iNOS@ZIF, the integration of both Pt NPs and iNOS enzyme exhibited better catalytic activities of NO production. Additionally, a positive correlation between NO level and the loading amount of Pt NPs was obtained (Fig. 3f). To evaluate the overall antioxidant capacity of the as-prepared Pt-iNOS@ZIF nanoreactor, the 2,2'-Azino-bis(3-Ethylbenzothiazoline-6-Sulfonic Acid) (ABTS) assay was performed based on the reduction of $ABTS^{\bullet+}$ radicals by antioxidants (Fig. 3g). As shown in Fig. 3h, the $ABTS^{\bullet+}$ radicals with blue color exhibited obvious absorbance decrease and discoloration in the presence of Pt-iNOS@ZIF. Also, the radical scavenging efficiency is positively related to the nanoparticle concentrations, implying favorable antioxidant ability of Pt-iNOS@ZIF to scavenge ATBS radicals (Fig. 3i).

Cellular evaluation of Pt-iNOS@ZIF. Next, we examined the antioxidant effects of Pt-iNOS@ZIF in primary mouse hepatocyte FL38B cells. H_2O_2 was utilized to stimulate intracellular oxidative stress and 2',7'-dichlorofluorescein diacetate (DCFH-DA) was applied as ROS indicator. As shown in Fig. 4a, strong green fluorescence signals were observed with the addition of H_2O_2 as compared to the control group without H_2O_2 treatment. When treated with Pt@ZIF or Pt-iNOS@ZIF, the intracellular fluorescence signals were

remarkably decreased, while there was minimal fluorescence disturbance in the ZIF-8 NPs treated group. Quantitative analysis by flow cytometry revealed reduced intracellular ROS level (51.4%) in (Pt@ZIF + H_2O_2)-treated cells as compared to that in H_2O_2-stimulated cells (59.1%), suggesting the ROS scavenging effect from Pt nanozyme. As comparison, Pt-iNOS@ZIF treated group remarkably decreased ROS level to around 22.8% in H_2O_2-pretreated cells (**Supplementary Fig. S3**). Moreover, the Pt-iNOS@ZIF exhibited concentration-dependent inhibition of ROS generation (Fig. 4c). Subsequently, intracellular NO levels were evaluated by the nitric oxide indicator (DAF-FM diacetate) *via* flow cytometry analysis and Pt-iNOS@ZIF + H_2O_2 group exhibited stronger fluorescence signals than the other groups (Fig. 4b). Then the protective effect of Pt-iNOS@ZIF against H_2O_2-induced oxidative stress in cells was evaluated by the standard methyl thiazolyl tetrazolium (MTT) assay. Unsurprisingly, H_2O_2 (250 μM) treatment resulted in about 41% cell death after incubation for 24 h, while the addition of Pt-iNOS@ZIF exhibited concentration-dependent increase of the cell viability, implying its protective effect against oxidative damage (Fig. 4d). Moreover, all designed NPs would induce negligible cell death in hepatocyte, HEK 293 cells and macrophage cells (up to 40 μg/mL), suggesting their good biocompatibility and minimum side effect from the nanoformulas themselves (**Supplementary Fig. S4-S8**). Collectively, all these results demonstrated that Pt-iNOS@ZIF-8 NPs could effectively alleviate oxidative stress and rescue cells from ROS-induced damage.

***In vivo* imaging and biodistribution.** In comparison with small molecular drugs, various types of nanomaterials have intrinsic advantages of passive targeting and accumulation in the liver. To evaluate the biodistribution and liver accumulation of Pt-iNOS@ZIF in living systems, Cy5 labeled iNOS enzyme was applied to form Pt-iNOS (Cy5)@ZIF and real-time fluorescence imaging was carried out in mice after intravenous injection (i.v.) of the NPs. As shown in Fig. 5a and **Supplementary Fig. S9**, there was an obvious increase of fluorescence signals at 1 h post injection (p.i.) and semi-quantitative analysis revealed that the NPs could remain in the liver for up to 10 h (7.2×10^8 p/s/cm^2/sr) and were gradually cleared from the liver by 24 h (3.4×10^8 p/s/cm^2/sr) p.i. Moreover, the *ex vivo* biodistribution in major organs at 24 h verified by fluorescence imaging and ICP-OES demonstrated that the NPs were able to efficiently accumulate in the liver (22.84 ± 3.65%ID g^{-1}), serving as an optimal candidate for IRI intervention (Fig. 5b-d).

Protective effect in a hepatic IRI model. Based on the promising antioxidant effect of Pt-iNOS@ZIF, we further investigated the feasibility of the protective effect against IRI in a murine model. C57BL/6 mice were treated with different nanoplatforms for 12 h before the clamping of porta hepatis. After 60 min of ischemia and reperfusion, the blood and liver samples with various treatments were collected and liver functions were further evaluated at 12 h after surgery. Alanine aminotransferase (ALT) and aspartate aminotransferase (AST) levels were clinically applied as indicators of liver damage. Compared to the sham-operated control group, the IRI mice group displayed significant increase of ALT and AST levels, indicating alleviated liver injury. When the IRI mice were pretreated with different types of NPs, the Pt-iNOS@ZIF treated IRI mouse group had remarkably reduced ALT and AST levels compared to those in ZIF-8 NPs, Pt NPs and Pt@ZIF treated groups, clearly demonstrating the effective intervention of liver

injury by Pt-iNOS@ZIF (Fig. 5e and 5f). To further evaluate the therapeutic efficacy, hematoxylin and eosin (H&E) staining was performed in liver tissues after pretreatment with various NPs in IRI mice. As expected, severe hepatocyte necrosis and cytolysis was observed in the PBS-treated IRI group after 12 h. The ZIF-8 NPs, Pt NPs and Pt@ZIF NPs treated groups displayed indistinguishable difference in the liver injury. By contrast, Pt-iNOS@ZIF-treated IRI group remarkably reduced the hepatocyte damage, implying the effective prevention from IRI (Fig. 6a). Overall, the results were consistent with the trend of ALT and AST levels. Moreover, the difference between Pt-iNOS@ZIF treated IRI group after 7 days and the control group was marginal (**Supplementary Fig. S10)**. Besides the therapeutic effectiveness of the designed nanomedicine, the safety in living systems is also important for further potential clinic applications. Hemolysis test (24 h p.i.), profiles of liver and kidney functions, and H&E staining of major organs after injection of Pt-iNOS@ZIF for 7 days were evaluated (**Supplementary Fig. S11-S14)**. All results showed Pt-iNOS@ZIF exhibited excellent biocompatibility and could be considered as an ideal candidate for the prevention of IRI.

Liver IRI is a pathophysiological event and oxidative stress is considered as one essential mechanism. To further obtain visual evidence for cellular events, immunofluorescence imaging was performed on liver tissues. Results indicated that hepatic IRI led to obvious activation of monocytes/macrophages compared to the sham group. The designed Pt@ZIF NPs can slightly inhibit the activation of macrophages, likely due to its ROS scavenging effect (Fig. 6b). By employing both ROS scavenging derived from Pt nanozyme and NO-based modulating effect, Pt-iNOS@ZIF treated mice exhibited minimal activation of monocyte/macrophages. Similarly, the Pt-iNOS@ZIF treated group also greatly suppressed the recruitment of neutrophils and caspase activities for preventing cells from apoptosis compared to the IRI group (Fig. 6c and **Supplementary Fig. S15**). Taken together, all these findings indicated that the preconditioning of Pt-iNOS@ZIF could inhibits IRI-induced macrophage activation, neutrophil accumulation, and subsequent apoptotic processes.

Encouraged by the above results, we further investigated the anti-inflammatory activities of the designed Pt-iNOS@ZIF, the expression of mRNAs for the pro-inflammatory mediators, including interleukin-1 beta (IL-1β), interleukin-1α (IL-1α), interleukin-6 (IL-6), interleukin-12 (IL-12), tumor necrosis factor-α (TNF-α), and interferon gamma (INF-γ) were measured from each group. As shown in Fig. 7, the levels of these pro-inflammatory cytokines were significantly increased in the hepatic IRI group, while they were reduced to relatively normal ranges in Pt-iNOS@ZIF treated IRI group. TNF-α is one intensively studied cytokine in response to inflammatory and immunomodulatory stimuli, and is a regulator responsible for the production of ROS. Also, IL-1 can facilitate the synthesis of TNF-α by Kupffer cells and recruitment of neutrophils [37]. IFN-γ produced mainly by activated natural killer T cells will promotes Kupffer cells or dendritic cell activation. The Kupffer cells and neutrophil activation in turn will induce the release of various chemokines and cytokines, including TNF-α, IL-1β, IL-6, IL-12, *etc*.[38], which further activates local immune cells, recruits circulating immune cells and aggravates liver damage. Taken together, these results indicated that Pt-iNOS@ZIF preconditioning would significantly suppress the expression of proinflammatory cytokines, which is generally involved in the initiation and propagation of IRI.

Discussion

IRI include a series of complicated processes including the restriction of blood supply, subsequent restoration and reoxygenation, during which the imbalance of metabolic supply, inflammation and oxidative damage are involved. Additionally, the innate and adaptive immune responses will be activated, resulting in cell damage and organ dysfunction[2]. In-depth understanding of the molecular mechanisms of IRI and innovative intervention strategies will greatly improve the success of surgery and survival rate of patients. Oxidative stress is considered to play a pivotal role in ischemia and reperfusion damage. It has been reported that ROS scavenging *via* supplementation of antioxidants has the ability of diminishing oxidative stress and ensuing organ injury[39]. Antioxidant enzyme-SOD can promote the conversion of $\bullet O_2^-$ to O_2 and H_2O_2. Also, H_2O_2 can be decomposed to H_2O and O_2 under the catalysis of CAT. Therefore, both enzymes exhibited beneficial actions by accelerating the detoxification of ROS in IRI. However, the short half-life of these natural proteases in the body (half-life of SOD is about 6 min), difficulty of cell uptake, and low delivery efficiency hinder their further applications[8]. Besides, NO, one of therapeutic gaseous molecules, has multiple regulatory functions, such as improving the microcirculation, suppressing caspase activities, and inhibiting neutrophil infiltration and platelet aggregation[40]. NO-based therapy has been applied for pulmonary hypertension and cardiopulmonary disorders for many years[41], and its therapeutic effect on protection liver from IRI has increasingly received considerable attention[17,42]. Although many approaches have been explored in the prevention of IRI, there are still no ideal intervention strategies applied in clinical practice.

More recently, Pt nanozyme has attracted great interest as the substitute of natural enzymes[43,44]. In this study, we successfully synthesized ultrasmall Pt NPs, which could act as SOD and CAT mimics with excellent ROS scavenging capacity. In order to further enhance the therapeutic efficacy, NO-based therapy is incorporated by integrating the iNOS enzyme and Pt nanozyme into ZIF-8 architecture to achieve synergistic effect. Co-precipitation method was applied to obtain the hybrid nanoreactor, ensuring efficient embedding of iNOS into ZIF-8 during the process of nanoparticle formation. Such design not only prevents natural enzymes from inactivation and degradation in the body, but also promotes the molecular diffusion and intercommunication due to the intrinsic porous feature and large surface areas of metal-organic frameworks[45,46]. More importantly, as the synthesis of NO is O_2-dependent, the generated O_2 by Pt catalysis will further improve the iNOS-mediated cascade reaction activities. After the ischemia and reperfusion, the restoration of blood flow will cause the release of ROS, activation of macrophage cells and recruitment of neutrophils, which further leads to the release of large amount of chemokines and cytokines[2]. Apart from the ROS elimination by Pt nanozyme, protective actions of NO during ischemia and reperfusion are probably attributed to antioxidant and anti-inflammatory effects. The prepared Pt-iNOS@ZIF nanoreactor could maintain ALT and AST levels of IRI mice in the relatively normal range. Additionally, it greatly suppressed the activation of macrophages cells, along with the minimized infiltration of neutrophils and expression of pro-inflammatory cytokines, which eventually attenuated the liver damage caused by IRI.

In summary, we developed an ZIF-8-based hybrid nanoreactor, which encapsulated the Pt nanozyme and natural enzyme iNOS, for protecting the liver from IRI. By using the excessive ROS generated during hepatic ischemia/reperfusion as a stimulus, the Pt nanozyme with SOD/CAT-like properties could scavenge $\bullet O_2^-$ and H_2O_2 to produce O_2, which can further react with L-Arg to form NO under the catalysis of iNOS enzyme. Such designed cascade reaction successfully achieved the ROS scavenging ($\bullet O_2^-$ and H_2O_2) and NO production, which effectively reduced oxidative stress and expression of proinflammatory cytokines in the process of hepatic ischemia and reperfusion. Overall, this study may shed new light on dual protection mechanism of ROS clearance and NO regulation, which is beneficial to advance further clinical applications in hepatic IRI.

Methods

Syntheis of platnium nanoparticles (Pt NPs). The ultra-small platinum nanoparticles were prepared according to the reported method with slight modification[35]: Briefly, in 10 mL of 1 mM hexachloroplatinic acid hexahydrate ($H_2PtCl_6 \bullet 6H_2O$) solution, 111.1 mg of polyvinylpyrrolidone (PVP) was added. After stirring for 15 min, 200 μL freshly prepared sodium borohydride ($NaBH_4$) solution (100 mM) was added and stirred for 12 h. The solution turned dark brown and Pt NPs were obtained for further use.

Syntheis of ZIF-8, Pt@ZIF, Pt-iNOS@ZIF Nanosystms. The ZIF-8 nanoparticles were synthesized according to the previous method[36]. Briefly,100 μL $Zn(NO_3)_2 \bullet 6H_2O$ aqueous solution (0.5 M) was added into 900 μL 2-methylimidazole (2-MIN, 3.5 M) and the mixture was stirred at room temperature for 1 h. The obtained product was collected by centrifugation (8000 rpm, 10 min) and washed with water for three times. Similarly, nanoscale Pt@ZIF was synthesized by mixing the 50 μL Pt NP solution with 900 μL 2-methylimidazole, followed by the additon of $Zn(NO_3)_2 \bullet 6H_2O$, The resulting Pt@ZIF was redispersed in water for further use. To synthezie nanoscale Pt-iNOS@ZIF, 0.3 mg iNOS enzyme was incubated with 900 μL 2-MIN for 10 min at 30°C followed by addition of zinc nitrate. For the synthesis of Pt-iNOS(Cy5)@ZIF, 0.5 mg cyanine 5 NHS ester (Lumiprobe) was reacted with iNOS (0.3 mg) in PBS solution for overnight. Then the product was dialyzed to remove excessive dye molecules. The obtained iNOS (Cy5) was used to prepare Pt-iNOS(Cy5)@ZIF by using the same method for the synthesis of Pt-iNOS@ZIF. After centrifugation and washing with water for three times, the obtained products were characterized by transmission electron microscopy (TEM) and dynamic light scattering (DLS).

Assays of SOD-like and CAT-like activities. To evaluate the Pt nanozyme properties, the superoxide anion scavenging activity was conducted with a SOD assay kit (Sigma-Aldrich, USA). The hydrogen peroxide quenching activity was performed with the Amplex® red hydrogen peroxide assay kit (Sigma-Aldrich, USA). All expreiments were carried out according to the standard protocol. To monitor the O_2 production, different concentrations of Pt NPs (0.5, 1.0 and 2.0 μg/mL) were mixed with 10 mM H_2O_2 in PBS buffer (pH 7.4), the dissiolved oxygen levels over time were measured by a dissolved oxygen probe. To obtain the enzyme kinetic parameters, different concencentraions of H_2O_2 were incubated with Pt NPs (2.0

μg/mL) for 10 min, the Michaelis-Menten constant (K_M) and maximum velocity (V_{max}) were determined as following equation:

$$: v = \frac{V_{max} \cdot [S]}{[S]+K_m}.$$

In vitro **measurement of total antioxidant capacity.** The $ABTS^{\bullet+}$ radical scavenging assay was applied to evaluate the total antioxidant capacity of Pt-iNOS@ZIF. Briefly, 7 mM ABTS in deionized water was prepared and reacted with 2.45 mM potassium persulfate overnight. Then the solution turned dark blue and ABTS radical cation ($ABTS^{\bullet+}$) was obtained. Next, 200 μL diluted solution was mixed with different concentrations of Pt-iNOS@ZIF for 5 min and the UV-Vis spectra were recorded. The radical scavenging efficiency was calculated based on the absorbance changes at 734 nm.

Intracellular ROS and NO measurements. Intracellular ROS levels were measured using 2',7'-dichlorofluorescein diacetate (DCFH-DA) as the ROS indicator and NO levles were measured using nitric oxide indicators (DAF FM Diacetate). 8 μg/mL different types of NPs (ZIF-8, Pt@ZIF, Pt-iNOS@ZIF) were added into cells and cultured for 2 h, followed by the treatment with H_2O_2 (1 mM) and incubated for another 4 h at 37°C. Then, the cells were stained with DCFH-DA (10 μM) or DAF probe (5 μM) for 30 min. After removing the excessive probe, fluoresence images were acquired by confocal laser scanning microscopy (CLSM). H33342 channel (λ_{ex} = 408 nm), FITC channel (λ_{ex} = 488 nm). Quantative ROS levels with dfferent concentrations of Pt-iNOS@ZIF treatment (1, 2, 4, 8 μg/mL) were analyzed by flow cytometry.

Preparation of hepatic IRI model in mice. Male C57BL/6 mice (6–8 weeks old) were received from Zhejiang Experimental Animal Center and were fed with a standard diet and water. All animal laboratory operations were carried out according to the Guide of Animal Ethics Committee of Shanghai Skin Disease Hospital. For hepatic IRI model preparation, the mice were fasted for 12 h before the surgical operation. After the mice were anesthetized with isoflurane, they were placed on a heated surgical pad and the abdomen of the depilated mice was disinfected with iodophor solution. Then a midline laparotomy was performed to expose the portal triplet. The portal triplet was carefully lifted using a vessel forceps, and all structures in the portal triplet (hepatic artery, portal vein, and bile duct) were blocked using a microvascular clamp. The abdominal wall was covered with PBS-soaked gauze and the blocking process lasted 60 min. After 60 min, microvascular clamp was removed for reperfusion. Signs of the reperfusion can be observed by the immediate color change of the central lobe and the left lobe of the liver.

In vivo **imaging and biodistribution.** For the fluorescence imaging, 100 μL Cy5-labled nanocomposite (Pt-iNOS(Cy5)@ZIF, 2 mg/kg) solutions was intravenously injected into male C57BL/6 mice (6–8 weeks old). In vivo fluorescence imaging was recorded at 1, 4, 10 and 24 h p.i. on an IVIS Spectrum system. At 24 h post injection, the above mice were sacrificed, and major organs were collected and washed before optical imaging. The fluorescence intensity of livers was acquired from the analysis of the region of interest (ROI) using a Living Image software.

Protective effect in a hepatic IRI model. The mice were randomly divided into six groups (n = 5) different formulations: (1) Sham, (2) PBS + IRI, (3) ZIF-8 + IRI, (4) Pt NPs + IRI, (5) Pt@ZIF + IRI, (6) Pt-iNOS@ZIF + IRI. Nanoformulations (2 mg/kg) in each group were intravenously injected 12 h before surgical operation. After 12 h induction of the hepatic IRI model in mice, the blood was collected for biochemical analysis. Liver and kidney functions were evaluated by blood tests of alanine aminotransferase (ALT) levels and aspartate aminotransferase (AST) levels (Shanghai Institute of Materia Medica, Center of Drug Safety Evaluation Research, CDSER, SIMM).The left liver lobes were dissected for hematoxylin and eosin (H&E) and immunofluorescence staining.

Immunofluorescence staining. Frozen tissue sections were prepared and covered with OCT media. Then the liver tissue sections were fixed with zinc fixative solutions for 10 min. After rinsing slides with PBS for 3 times, the liver tissues were further treated with 2% Triton X-100 for 15 min. Then 100 μL blocking buffer (10% FBS in PBS) was added onto tissues for 1 h. Antibodies including F4/80, CD31, Ly6G and caspase-3 were diluted and added on slides and incubated for overnight at 4°C. To stain the secondary antibody, slides were washed and incubated with secondary antibody conjugated with Alex 488 or 594 for 1 h. After that, the slides were rinsed with PBS and mounted with DAPI-containing mounting solution. Fluorescence images were acquired *via* confocal microscopy.

Measurement of inflammatory cytokine levels in liver tissues. To evaluate inflammatory cytokine levels,the left liver lobe tissues in each group were harvested at 12 h after surgery to detect the relative mRNA expression of IL-1α, IL-1β, TNF-α, IFN-γ, IL-12 and IL-6 using quantitative real-time polymerase chain reaction (qPCR) assay. Total RNA was extracted from the obtained liver tissues and reverse transcripted into cDNA in a gradient RNA apparatus. Subsequently, fluorescence qPCR amplification was performed and the relative mRNA expression levels of the cytokines mentioned above were measured and calculated.

Statistical analysis

Quantitative data were presented as mean ± s.d. Statistical differences were calculated by an unpaired two-tailed Student's t-test using Excel and A One-way analysis of the variance (ANOVA) using GraphPad Prism software. P values < 0.05 were considered statistically significant and illustrated by *P < 0.05, ** P < 0.01, *** P < 0.001, respectively.

Declarations

Data availability

The authors declare that the data supporting the findings of this study are available within the Article and its Supplementary Information Files or from the corresponding author upon reasonable request.

Acknowledgements

This work was financially supported by the Basic Research Program of Shenzhen (JCYJ20180305163622079), National University of Singapore Start-up Grant (NUHSRO/2020/133/Startup/08) and NUS School of Medicine Nanomedicine Translational Research Programme (NUHSRO/2021/034/TRP/09/Nanomedicine). All animal experiments were conducted according to the Guide of Animal Ethics Committee of Shanghai Skin Disease Hospital and the Animal Ethical and Welfare Committee of Shenzhen University (AEWC-SZU).

Author contributions

J. M., L. H., P. H., Y. Y., and X. C. conceived and designed the project. J. M., L. H., G. L., and J. Z. performed the material synthesis and characterizations. D. Z. and C. J. performed the XRD and elemental mapping studies. J. M., Y. S. performed the cell studies. J. M., C. L., and L. H. performed the animal studies. J. M., C. L., X. W., P. H., and Y. Y. analyzed animal results. J. M., C. L., L. H., P. H., Y. Y., and X. C. analyzed the results and co-wrote the paper. All the authors have discussed the results and approved the final version.

Competing interests

The authors declare no competing interests.

Additional information

Supplementary Information for this paper is available at www.nature.com/xxx.

References

1. Asrani, S.K., Devarbhavi, H., Eaton, J. & Kamath, P.S. Burden of liver diseases in the world. *J. Hepatol.* **70**, 151-171 (2019).

2. Eltzschig, H.K. & Eckle, T. Ischemia and reperfusion-from mechanism to translation. *Nat. Med.* **17**, 1391-1401 (2011).

3. Monga, S.P. Lipid metabolic reprogramming in hepatic ischemia-reperfusion injury. *Nat. Med.* **24**, 6-7 (2018).

4. Froghi, F., Froghi, S. & Davidson, B.R. Liver sschaemia-reperfusion Injury. *Liver Diseases* 129-141 (2020).

5. Zhai, Y., Petrowsky, H., Hong, J.C., Busuttil, R.W. & Kupiec-Weglinski, J.W. Ischaemia-reperfusion injury in liver transplantation-from bench to bedside. *Nat. Rev. Gastroenterol. Hepatol.* **10**, 79-89 (2013).

6. Davidson, S.M.*, et al.* Multitarget strategies to reduce myocardial ischemia/reperfusion injury: JACC review topic of the week. *J. Am. Coll. Cardiol.* **73**, 89-99 (2019).

7. Dar, W.A., Sullivan, E., Bynon, J.S., Eltzschig, H. & Ju, C. Ischaemia reperfusion injury in liver transplantation: Cellular and molecular mechanisms. *Liver Int.* **39**, 788-801 (2019).

8. Cannistrà, M.*, et al.* Hepatic ischemia reperfusion injury: A systematic review of literature and the role of current drugs and biomarkers. *Int. J. Surg.* **33**, S57-S70 (2016).

9. Li, S., Li, H., Xu, X., Saw, P.E. & Zhang, L. Nanocarrier-mediated antioxidant delivery for liver diseases. *Theranostics* **10**, 1262-1280 (2020).

10. Ni, D.*, et al.* Ceria nanoparticles meet hepatic ischemia-reperfusion injury: the perfect imperfection. *Adv. Mater.* **31**, 1902956 (2019).

11. Park, J.*, et al.* In situ electrochemical generation of nitric oxide for neuronal modulation. *Nat. Nanotechnol.* **15**, 690-697 (2020).

12. Midgley, A.C., Wei, Y., Li, Z., Kong, D. & Zhao, Q. Nitric-oxide-releasing biomaterial regulation of the stem cell microenvironment in regenerative medicine. *Adv. Mater.* **32**, 1805818 (2020).

13. Carpenter, A.W. & Schoenfisch, M.H. Nitric oxide release: Part II. Therapeutic applications. *Chem. Soc. Rev.* **41**, 3742-3752 (2012).

14. Hou, J.*, et al.* Targeted delivery of nitric oxide via a 'bump-and-hole'-based enzyme-prodrug pair. *Nat. Chem. Biol.* **15**, 151-160 (2019).

15. Huang, Z., Fu, J. & Zhang, Y. Nitric oxide donor-based cancer therapy: advances and prospects. *J. Med. Chem.* **60**, 7617-7635 (2017).

16. Duranski, M.R.*, et al.* Cytoprotective effects of nitrite during in vivo ischemia-reperfusion of the heart and liver. *J. Clin. Investig.* **115**, 1232-1240 (2005).

17. Fu, P. & Li, W. Nitric oxide in liver ischemia-reperfusion injury. *Liver Pathophysiology* 125-127 (2017).

18. Bhatraju, P., Crawford, J., Hall, M. & Lang Jr, J.D. Inhaled nitric oxide: current clinical concepts. *Nitric Oxide* **50**, 114-128 (2015).

19. Gao, L.*, et al.* Intrinsic peroxidase-like activity of ferromagnetic nanoparticles. *Nat. Nanotechnol.* **2**, 577-583 (2007).

20. Huang, Y., Ren, J. & Qu, X. Nanozymes: classification, catalytic mechanisms, activity regulation, and applications. *Chem. Rev.* **119**, 4357-4412 (2019).

21. Wu, J.*, et al.* Nanomaterials with enzyme-like characteristics (nanozymes): next-generation artificial enzymes (II). *Chem. Soc. Rev.* **48**, 1004-1076 (2019).

22. Jiao, L.*, et al.* When nanozymes meet single-atom catalysis. *Angew. Chem.* **132**, 2585-2596 (2020).

23. Jiang, D.*, et al.* DNA origami nanostructures can exhibit preferential renal uptake and alleviate acute kidney injury. *Nat. Biomed. Eng.* **2**, 865-877 (2018).

24. Fan, K.*, et al.* In vivo guiding nitrogen-doped carbon nanozyme for tumor catalytic therapy. *Nat. Commun.* **9**, 1-11 (2018).

25. Han, S.I.*, et al.* Epitaxially strained CeO_2/Mn_3O_4 nanocrystals as an enhanced antioxidant for radioprotection. *Adv. Mater.* **32**, 2001566 (2020).

26. Jiang, D.*, et al.* Nanozyme: new horizons for responsive biomedical applications. *Chem. Soc. Rev.* **48**, 3683-3704 (2019).

27. Wu, H.*, et al.* Bioactive ROS-scavenging nanozymes for regenerative medicine: Reestablishing the antioxidant firewall. *Nano Select* **1**, 285-297 (2020).

28. Kim, J.Y.*, et al.* Bilirubin nanoparticle preconditioning protects against hepatic ischemia-reperfusion injury. *Biomaterials* **133**, 1-10 (2017).

29. Yang, B., Chen, Y. & Shi, J. Reactive oxygen species (ROS)-based nanomedicine. *Chem. Rev.* **119**, 4881-4985 (2019).

30. Zhang, Y.*, et al.* Biomimetic design of mitochondria-targeted hybrid nanozymes as superoxide scavengers. *Adv. Mater.* **33**, 2006570 (2021).

31. Xu, Y.*, et al.* Nanozyme-catalyzed cascade reactions for mitochondria-mimicking oxidative phosphorylation. *Angew. Chem. Int. Ed.* **58**, 5572-5576 (2019).

32. Huo, M., Wang, L., Chen, Y. & Shi, J. Tumor-selective catalytic nanomedicine by nanocatalyst delivery. *Nat. Commun.* **8**, 1-12 (2017).

33. Cai, X.*, et al.* Nanozyme-involved biomimetic cascade catalysis for biomedical applications. *Mater. Today* **44**, 211-228 (2021).

34. Liu, Y.*, et al.* Integrated cascade nanozyme catalyzes in vivo ROS scavenging for anti-inflammatory therapy. *Sci. Adv.* **6**, eabb2695 (2020).

35. Teranishi, T., Hosoe, M., Tanaka, T. & Miyake, M. Size control of monodispersed Pt nanoparticles and their 2D organization by electrophoretic deposition. *J. Phys. Chem. B* **103**, 3818-3827 (1999).

36. Pan, Y., Liu, Y., Zeng, G., Zhao, L. & Lai, Z. Rapid synthesis of zeolitic imidazolate framework-8 (ZIF-8) nanocrystals in an aqueous system. *Chem. Commun.* **47**, 2071-2073 (2011).

37. Brenner, D., Blaser, H. & Mak, T.W. Regulation of tumour necrosis factor signalling: live or let die. *Nat. Rev. Immunol.* **15**, 362-374 (2015).

38. Roland, C.R., Walp, L., Stack, R.M. & Flye, M.W. Outcome of Kupffer cell antigen presentation to a cloned murine Th1 lymphocyte depends on the inducibility of nitric oxide synthase by IFN-gamma. *J. Immunol.* **153**, 5453-5464 (1994).

39. Cuzzocrea, S., Riley, D.P., Caputi, A.P. & Salvemini, D. Antioxidant therapy: a new pharmacological approach in shock, inflammation, and ischemia/reperfusion injury. *Pharmacol. Rev.* **53**, 135-159 (2001).

40. Coleman, J.W. Nitric oxide in immunity and inflammation. *Int. Immunopharmacol.* **1**, 1397-1406 (2001).

41. Ambalavanan, N., John, E.S., Carlo, W.A., Bulger, A. & Philips, J.B. Feasibility of nitric oxide administration by oxygen hood in neonatal pulmonary hypertension. *J Perinatol.* **22**, 50-56 (2002).

42. Lang, J.D.*, et al.* Inhaled NO accelerates restoration of liver function in adults following orthotopic liver transplantation. *J. Clin. Investig.* **117**, 2583-2591 (2007).

43. Zhang, D.-Y.*, et al.* Ultrasmall platinum nanozymes as broad-spectrum antioxidants for theranostic application in acute kidney injury. *Chem. Eng. J.* **409**, 127371 (2021).

44. Zhang, Y.*, et al.* Nanozyme decorated metal-organic frameworks for enhanced photodynamic therapy. *ACS Nano* **12**, 651-661 (2018).

45. Mu, J., He, L., Huang, P. & Chen, X. Engineering of nanoscale coordination polymers with biomolecules for advanced applications. *Coord. Chem. Rev.* **399**, 213039 (2019).

46. Chen, T.-T., Yi, J.-T., Zhao, Y.-Y. & Chu, X. Biomineralized metal-organic framework nanoparticles enable intracellular delivery and endo-lysosomal release of native active proteins. *J. Am. Chem. Soc.* **140**, 9912-9920 (2018).

Figures

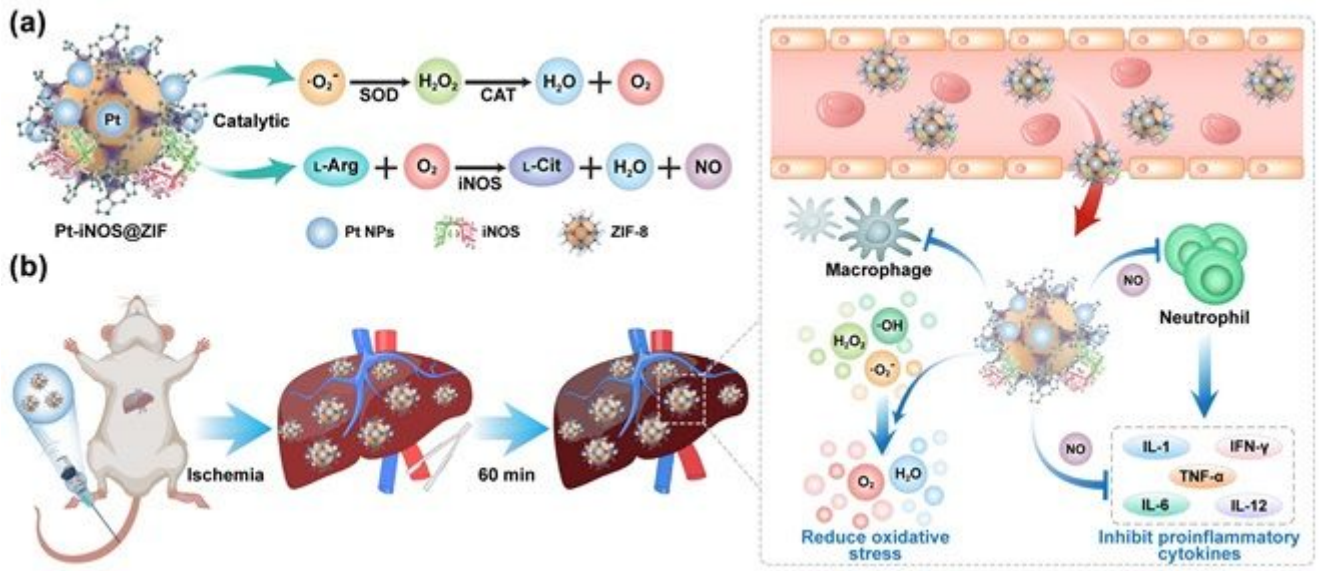

Figure 1

Schematic illustration of hepatic IRI prevention performance by Pt-iNOS@ZIF nanoreactor. a, Illustration of the designed Pt-iNOS@ZIF nanoreactor. The synthesized Pt nanozyme with SOD/CAT-like properties could scavenge overexpressed ROS induced by IRI to generate O2. Then iNOS enzyme could further catalyze 𝖫-Arginine (𝖫-Arg) and O2. to produce 𝖫-Citrulline (𝖫-Cit) and NO. b, Schematic of the hepatic IRI generation and treatment with the Pt-iNOS@ZIF nanoreactor. It can reduce oxidative stress and inhibit proinflammatory cytokines, resulting in effective prevention the liver from IRI.

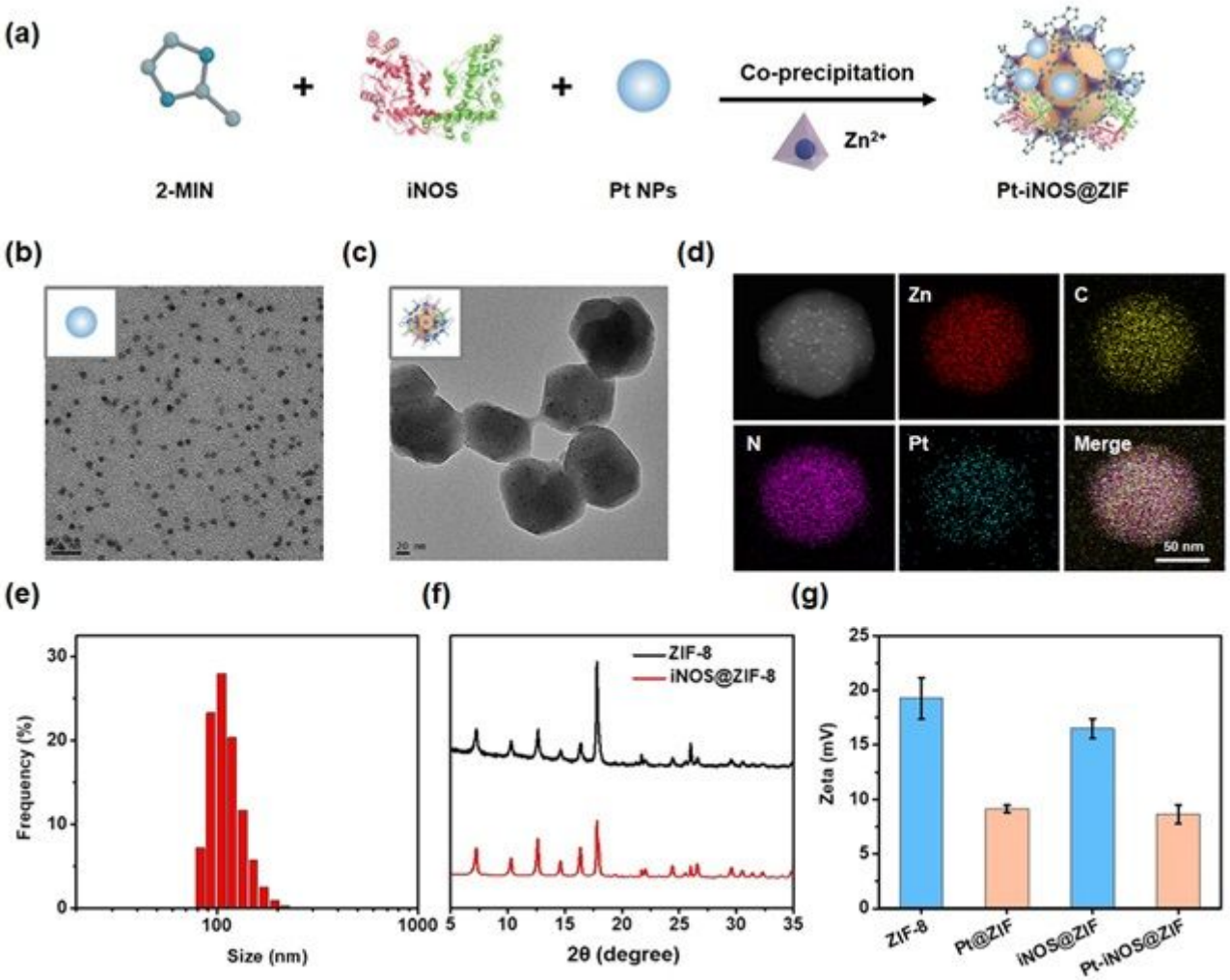

Figure 2

Preparation and characterizations of Pt-iNOS@ZIF nanoreactor. a, Synthetic procedure of Pt-iNOS@ZIF nanoreactor. b-c, TEM images of the synthesized Pt NPs and Pt-iNOS@ZIF nanoreactor. d-e, Elemental mapping and size distribution of Pt-iNOS@ZIF nanoreactor analyzed by dynamic laser scattering (DLS), scale bar: 50 nm. f, X-ray diffraction (XRD) patterns of ZIF-8 and iNOS@ZIF-8 NPs. f, Zeta potentials of different NPs (ZIF-8, Pt@ZIF, iNOS@ZIF and Pt-iNOS@ZIF).

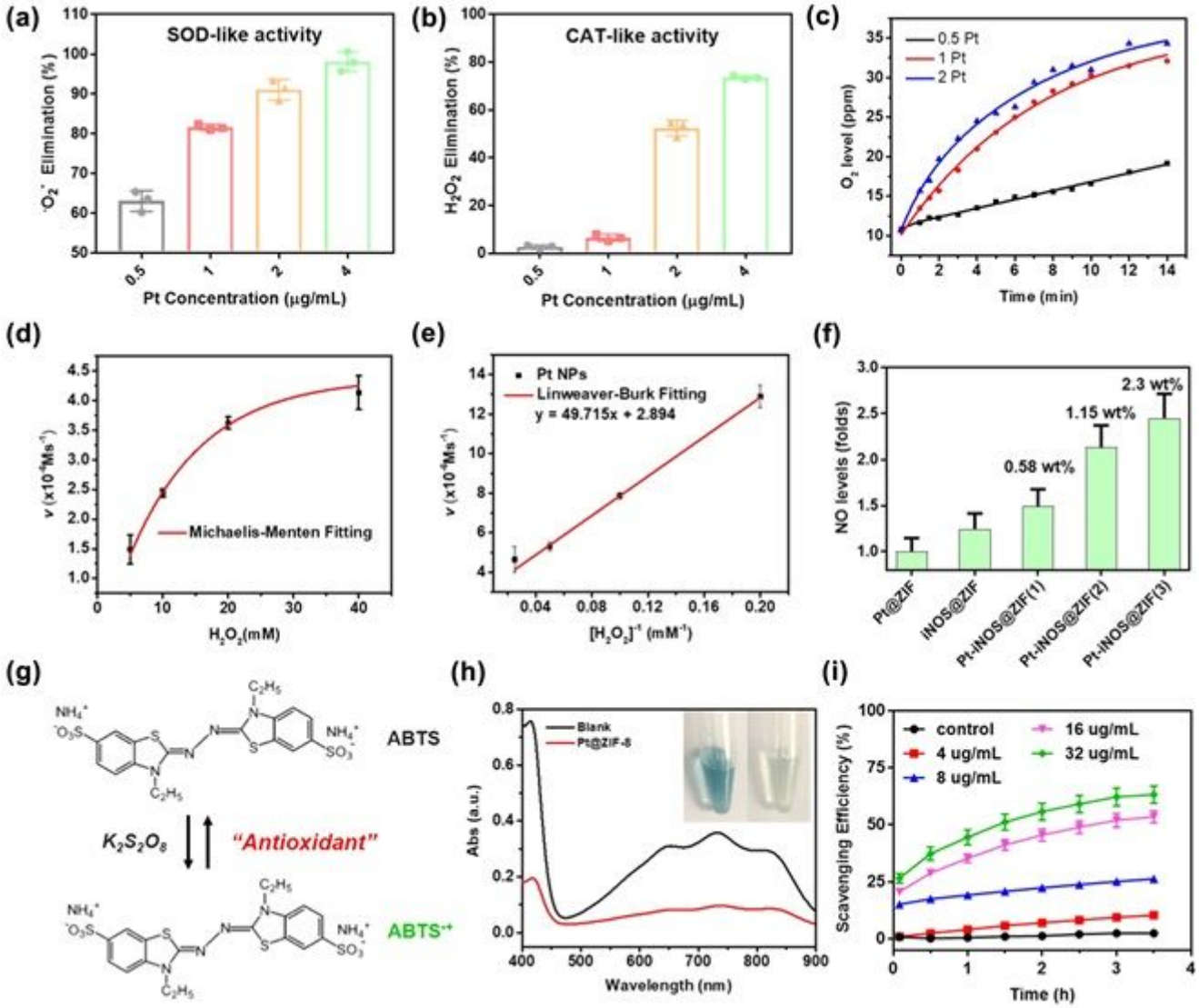

Figure 3

In vitro catalytic performance. a, b, ROS scavenging activities of Pt NPs with SOD-like and CAT-like properties. c, Concentration-dependent generation of O2 in the presence of Pt nanozyme. d, e, Michaelis-Menten steady-state kinetics of O2 generation from the decomposition of H2O2 by Pt NPs. f, The generation of NO by the Griess assay with the increase of Pt loading content (0.58, 1.15, 2.3 wt%). g, The antioxidant principle of the ABTS assay. h, Absorbance and pictures of ABTS radicals with or without treatment of Pt-iNOS@ZIF at 3 h. i, Analysis of the scavenging efficiency of ABTS radicals by different concentrations of Pt-iNOS@ZIF.

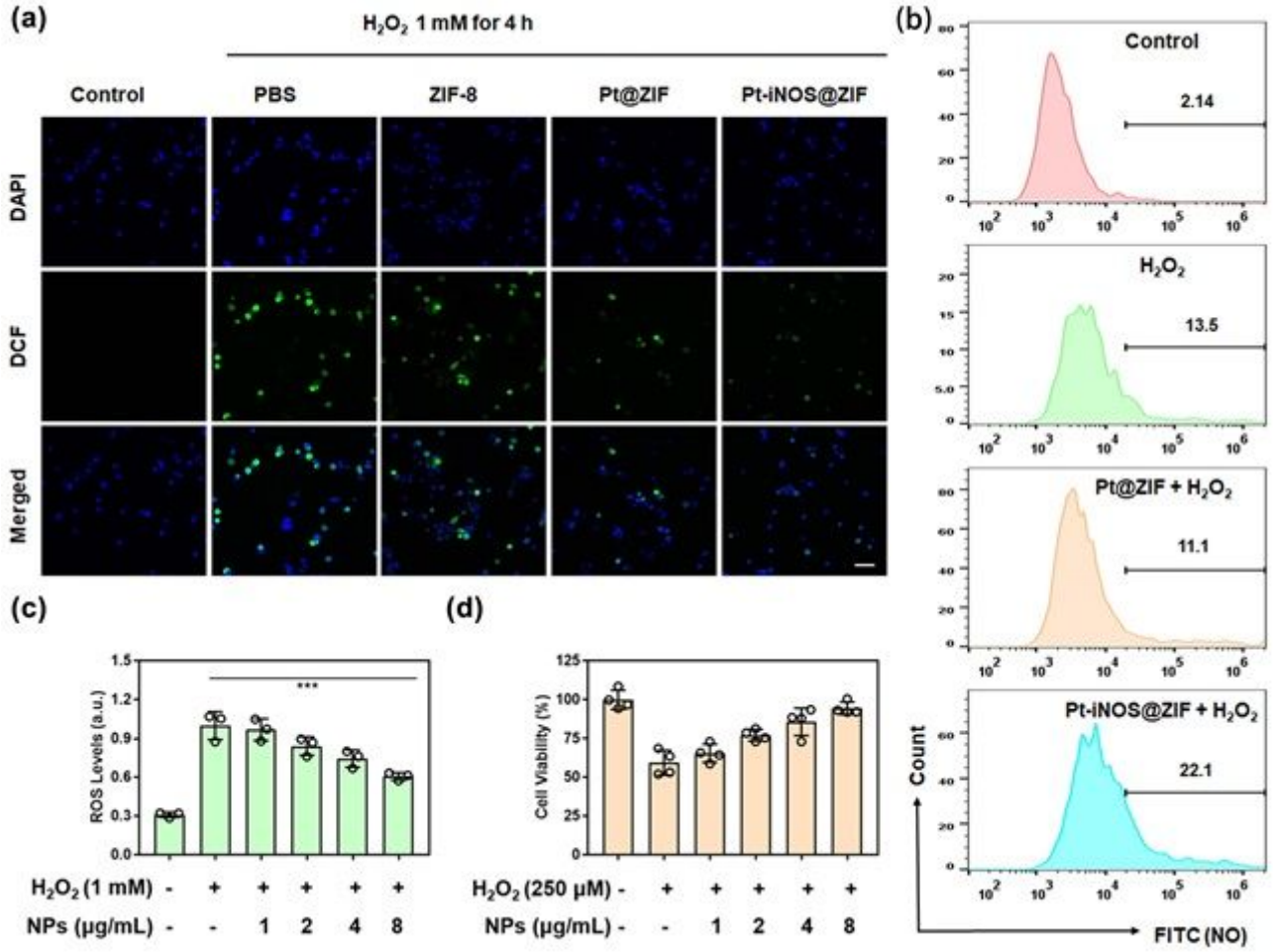

Figure 4

Antioxidant and cell protection activities in FL38B cells. a, Fluorescence images of ROS levels in H2O2-stimulated hepatocytes pretreated with PBS, ZIF-8, Pt-ZIF and Pt-iNOS@ZIF NPs (8 μg/mL). Cells were stained with DCFH-DA (green) and Hoechst 33342 (blue) after 4 h incubation. Scale bar: 50 μm. b, Flow cytometry analysis of NO levels with various treatments. c, ROS levels H2O2-stimulated hepatocytes pretreated with different concentrations of Pt-iNOS@ZIF (0, 1, 2, 4, 8 μg/mL). d, Cell viability in hepatocytes stimulated with H2O2 for 24 h in the presence of Pt-iNOS@ZIF (0, 1, 2, 4, 8 μg/mL). Data presented as means ± s.d. * $P < 0.05$; ** $P < 0.01$, *** $P < 0.001$

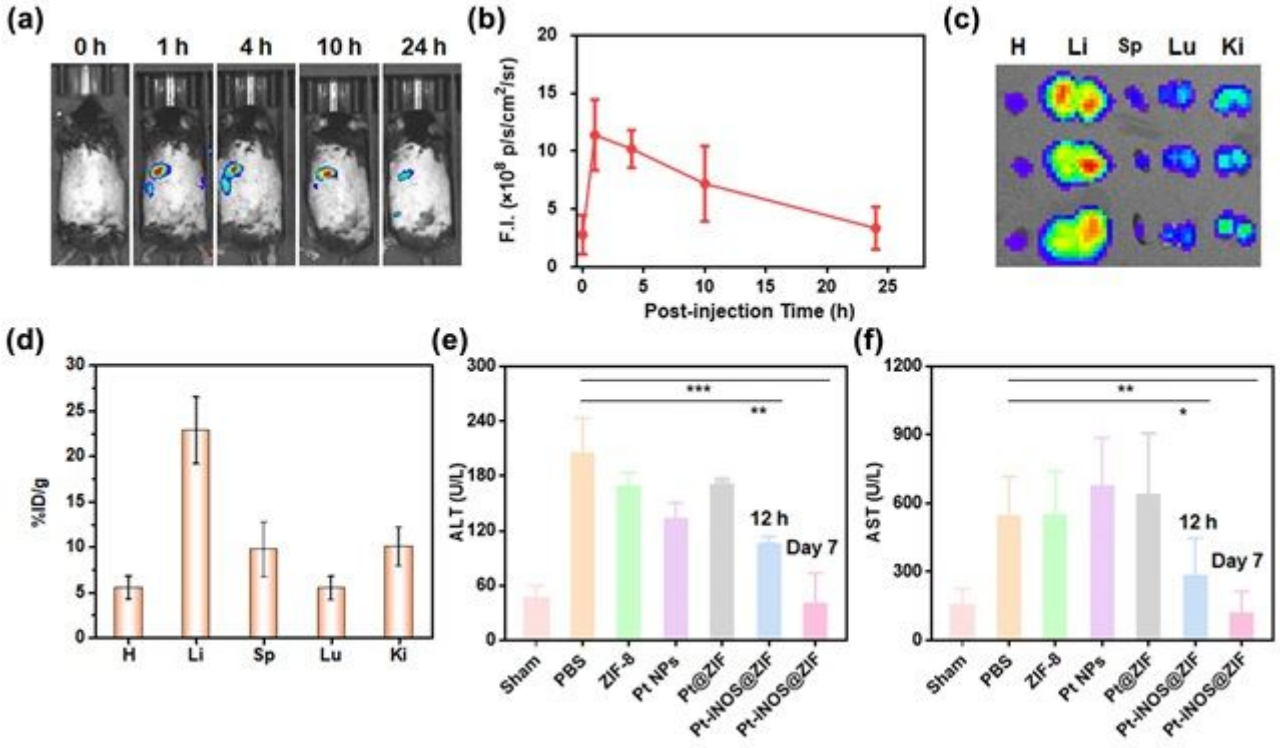

Figure 5

In vivo performance. a, Representative in vivo fluorescence images of C57BL/6 mice at 1, 4, 10, and 24 h p.i. of Pt-iNOS@ZIF (n = 3). b, Quantitative ROI assays of the fluorescence intensity in mice at designated time points. c, Ex vivo fluorescence images of major organs at 24 h p.i. H: heart, Li: liver, Sp: spleen, Lu: lung, Ki: kidney. d, Biodistribution of Pt-iNOS@ZIF in major organs at 24 h p.i. evaluated by ICP-OES. e, f, Serum ALT and AST levels in mice after 60 min of ischemia and 12 h of reperfusion from each group. Data presented as means ± s.d. * $P < 0.05$; ** $P < 0.01$, *** $P < 0.001$

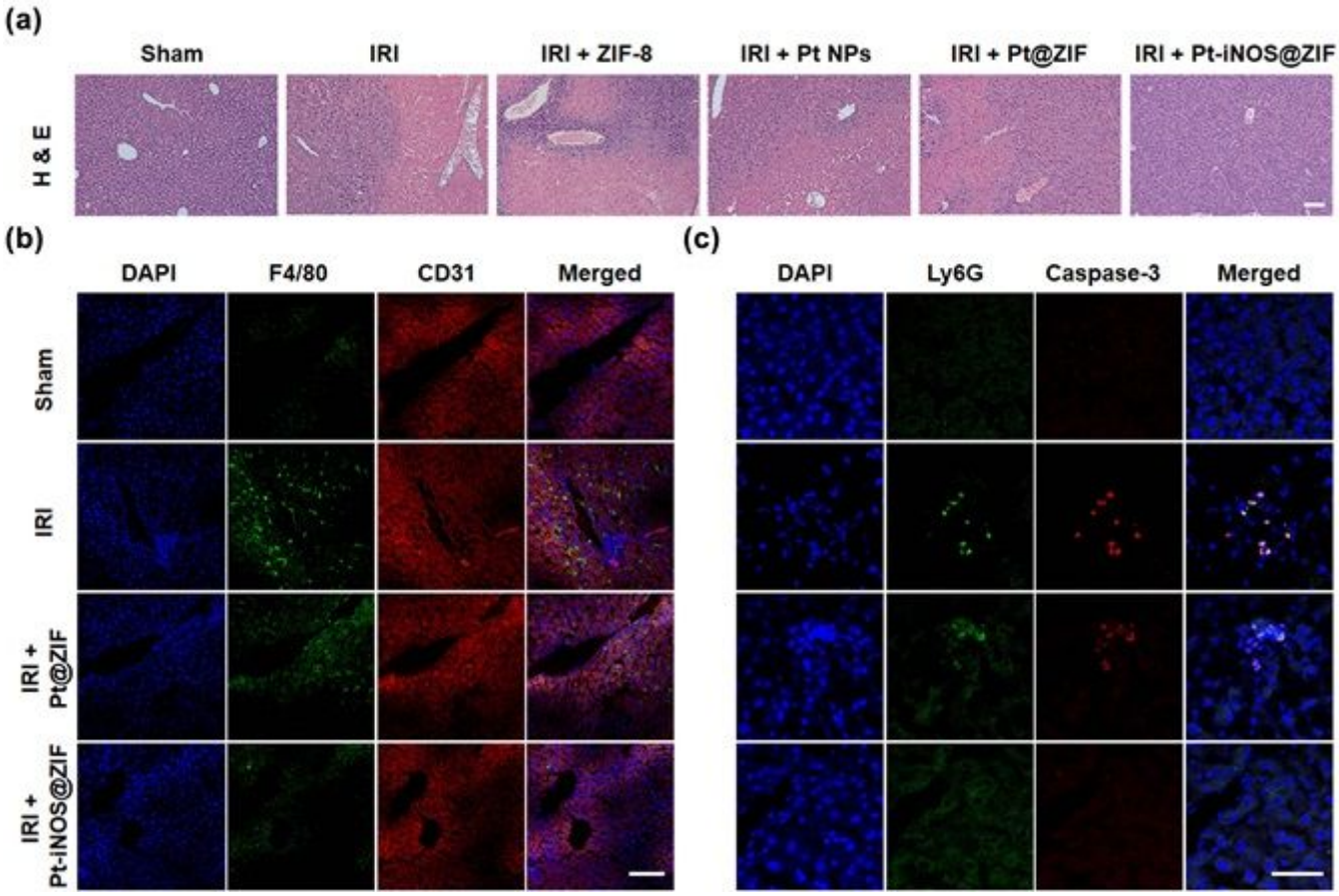

Figure 6

H&E and Immunofluorescence staining on liver tissues. a, H&E staining of liver tissues from each group (Sham, PBS, ZIF-8, Pt NPs, Pt@ZIF, Pt-iNOS@ZIF) after 60 min of ischemia and 12 h of reperfusion. Scale bar: 100 μm. b, Immunofluorescence staining of liver tissues with various treatments by using DAPI (blue) for nuclear staining, anti-F4/80 antibody (green) as monocyte/macrophage marker, and anti-CD31 antibody (red) as an endothelial marker from each group. Scale bar: 100 μm. c, Enlarged images of immunofluorescence staining with various treatments by using DAPI (blue) for nuclear staining, anti-Ly6G antibody (green) as neutrophil marker and anti-caspase-3 antibody (red) as a cell apoptosis marker. Scale bar: 50 μm.

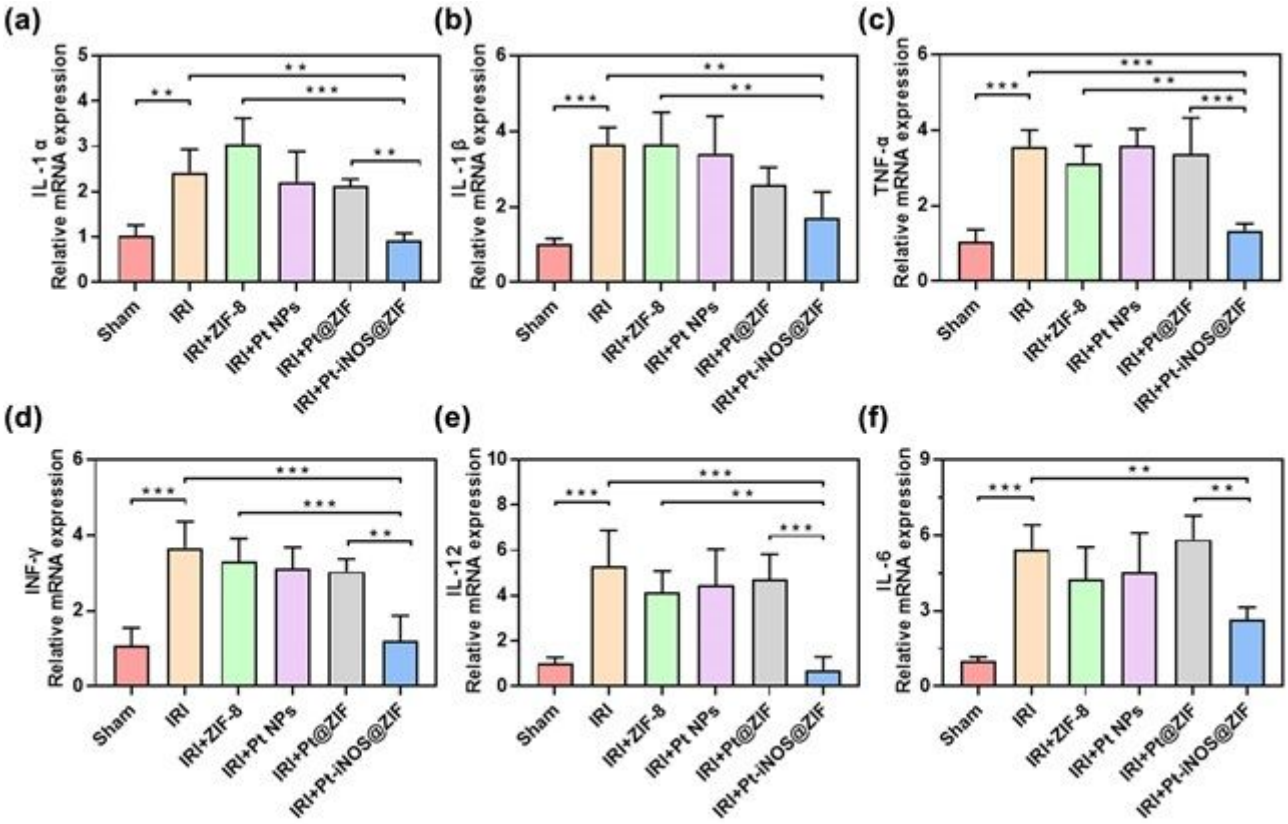

Figure 7

Anti-inflammatory activities in hepatic IRI. a-f, Relative expression of mRNAs for cytokines of IL-1α (a), IL-1β (b), INF-γ (c), IL-12α (d), TNF-α (e), IL-6 (f). Data presented as means ± s.d. from three independent replicates, and P values were calculated by one-way analysis of the variance (ANOVA). * $P < 0.05$; ** $P < 0.01$, *** $P < 0.001$.

Supplementary Files

This is a list of supplementary files associated with this preprint. Click to download.

- NatureCommSIJing6262021.docx
- nrreportingsummaryJing.pdf